III INTERNATIONAL CONGRESS ON COMPUTATIONAL BIOENGINEERING
M. Cerrolaza, H. Rodrigues, M. Doblaré, J. Ambrosio, M. Viceconti
(Eds.)
Isla de Margarita, Venezuela, September 17 to 19, 2007

SENSITIVITY OF BLOOD FLOW AT THE CAROTID ARTERY TO THE HEART INFLOW BOUNDARY CONDITION

P. J. Blanco*, M.R. Pivello*, R.A. Feijóo* and S. Urquiza**

* LNCC – Laboratório Nacional de Computação Científica. Av. Getúlio Vargas, 333, Quitandinha. 25651-075. Petrópolis, RJ, Brazil
e-mail: pjblanco@lncc.br, pivello@lncc.br, feij@lncc.br

** Laboratorio de Bioingeniería, Universidad Nacional de Mar del Plata, Av. J.B. Justo 4302, Mar del Plata, Argentina.
e-mail: santiagourquiza@fi.mdp.edu.ar

Keywords: Blood flow, Carotid Artery, Inflow boundary Condition, Coupled Models, FEM.

Abstract. *In this work we present a study on the influence of the heart inflow boundary condition on the blood flow patterns and on the arterial pulse conformation at the carotid artery. For this purpose, a 3D–1D coupled model for the simulation of the human cardiovascular system is used. The representation of the 1D arterial tree proposed by Avolio [1] is coupled with a 3D real model of the carotid artery acquired from a patient-specific MRI using image segmentation and reconstruction techniques. Different heart ejection curves are applied as the inflow boundary condition, and the local behavior of the blood flow in the carotid bifurcation is then analyzed. The main goal is to compare the flow patterns regarding recirculation regions by means of the computation of some well-known indicators, such as the OSI and WSS distributions.*

1 INTRODUCTION

The mathematical modeling of the Human Cardiovascular System helps to better understand the phenomena involved in the conformation of the arterial pulse at different districts of the arterial system [2,6]. However, because of the complexity of the system, simulating the whole arterial system with full 3D models is still an unfeasible task, and coupled 3D–1D models of the arterial system are usually employed instead [2,6]. A simplified version of the Navier–Stokes equations in compliant vessels represents the phenomena at the major arterial districts scale, whereas localized 3D models are used to study in detail the blood flow at regions of particular interest. In this way, the main goal of this work is to study the influence of the heart ejection curve, as the inflow boundary condition applied to the 1D portion of the model, on the characteristics of the hemodynamics at the carotid artery bifurcation. In this regard, quantities of interest defined on both 3D and 1D regions of the coupled model are compared. Specifically, the influence of five different flow ejection curves on the flow rate and pressure curves, as well as on local flow patterns at the carotid bifurcation and on indicators referring to the oscillating and average behavior of shear stresses, is studied.

2 THE MODEL

The governing equations were derived based on a variational formulation for the coupling of kinematically incompatible models, in this case 3D-1D flow models in compliant vessels [2]. Under certain conditions the associated Euler equations for a Newtonian fluid when coupling a 1D domain Ω_{1D} with a 3D region Ω_{3D} through a coupling interface Γ_C, and considering the ALE formulation over Ω_{3D}, are the following:

$$\rho A\frac{\partial \overline{u}}{\partial t}+\rho A\overline{u}\frac{\partial \overline{u}}{\partial z}=-A\frac{\partial p}{\partial z}-8\mu\overline{u}+f^{z} \qquad in \qquad \Omega_{1D}\times(0,T) \tag{1}$$

$$\rho\left.\frac{\partial \mathbf{u}}{\partial t}\right|_{Y}+\rho\nabla\mathbf{u}(\mathbf{u}-\mathbf{w})=-\nabla p+\mu\Delta\mathbf{u}+\mathbf{f} \quad in \quad \Omega_{3D}\times(0,T) \tag{2}$$

$$\frac{\partial A}{\partial t}+\frac{\partial(A\overline{u})}{\partial t}=0 \quad in \qquad \Omega_{1D}\times(0,T) \tag{3}$$

$$\nabla\cdot\mathbf{u}=0 \quad in \qquad \Omega_{3D}\times(0,T) \tag{4}$$

$$\left(-p\mathbf{I}+2\mu\varepsilon(\mathbf{u})\right)\mathbf{n}_1=-\overline{p}\mathbf{n}_1 \quad in \quad \Omega_{3D}\times(0,T) \tag{5}$$

$$A_C\overline{u}=\int_{\Gamma_c}\mathbf{u}\cdot\mathbf{n}_1 d\Gamma \quad on \quad \Gamma_C\times(0,T) \tag{6}$$

Equations 1 and 3 represent the 1D model, and $\overline{u}$, $\overline{p}$ are the mean velocity and pressure values, ρ is the blood density, μ is the dynamic viscosity, A denotes the cross sectional area, $A\overline{u}$ is the flow rate and z is the axial coordinate. Equations 2 and 4 represent the 3D model, **u** is the blood velocity, **w** is the domain velocity consistent with the ALE framework and p is the blood pressure. Equation 5 stands for the continuity of the traction vector at Γ_C (the coupling interface between the 3D and 1D models), while expression 6 is the counterpart of the mass conservation, and $\mathbf{n}_1$ is the unit outward normal to domain Ω_{1D} over the coupling interface Γ_C.

The wall movement on Γ_w is modeled according to the independent ring model [2,6], and its equations are stated bellow:

$$\overline{p} = \overline{p}_o + \frac{E\pi R_o h_o}{A}\left(\sqrt{\frac{A}{A_0}} - 1\right) + \frac{k\pi R_0 h_0}{A}\frac{1}{2\sqrt{A_0 A}}\frac{dA}{dt} \quad in \quad \Omega_{1D} \times (0,T) \tag{7}$$

$$\overline{p} = \overline{p}_o + \frac{Eh}{R_0^2}\zeta + \frac{kh}{R_0^2}\frac{d\zeta}{dt} \quad in \quad \Gamma_w \times (0,T) \tag{8}$$

The deformation of the domain Ω_{3D} is accounted for through a laplacian problem, i.e., $\Delta\mathbf{d} = 0$ in $\Omega_{3D} \times (0,T)$. Since it is a small amplitude movement, no remeshing is performed. Instead, the laplacian problem is used to extend the wall movement to the interior of Ω_{3D}, and $\mathbf{d}|_{\Gamma w} = \zeta\mathbf{n}$ is the wall displacement, where ζ is the scalar field that denotes the displacement of the wall in the normal direction, given by **n**, that is obtained from eq. 8.

3. NUMERICAL APROXIMATION

In this section the numerical aspects of this work are briefly described, and details concerning the numerical techniques applied and the setting of the model regarding boundary conditions as well as the 3D geometry and the 1D arterial network topology are given.

Time discretization is performed with a single step finite difference method corresponding to a classical θ scheme for both 1D and 3D parts. The spatial discretization is carried out through the Finite Element Method. In particular, the 1D model is written in conservative form and in its canonical form. Variables Q, A, $\overline{p}$ of the 1D model are discretized with P_1 finite elements, while **u**, p in the 3D model are discretized with $P_1^B - P_1$ finite elements. The index B stands for bubble functions for the velocity field according to the *mini element* formulation. The domain displacement **d** is also approximated with P_1 finite elements, and the reference velocity **w** is computed from the displacement by a backward Euler difference scheme. For both 1D and 3D parts, stabilization terms are included in order to avoid non–physical oscillating solutions present in standard Galerkin approximations. In the 1D model these terms are incorporated along the characteristics lines and correspond to a Galerkin Least Squares formulation. In the 3D model the stabilization terms correspond to the SUPG technique. Nonlinearities are treated with Picard iterations.

Numerical tests were performed using the 1D model of the arterial tree proposed by Avolio

[1]. The carotid artery geometry, obtained via segmentation of MRI images, was discretized with a mesh of tetrahedra. Figure 1-left shows the topology of the arterial tree and the location of the embedding of the 3D district within the 1D model. Five flow curves for the cardiac ejection were tested as inflow boundary condition for the 1D model to assess their influence on the flow behavior on both 1D and 3D portions of the model. In all cases, the blood flow rate is 5 l/min and the cardiac period is T = 0.8 sec. Figure 1-right shows the flow rate versus time in a cardiac cycle, according to different works.

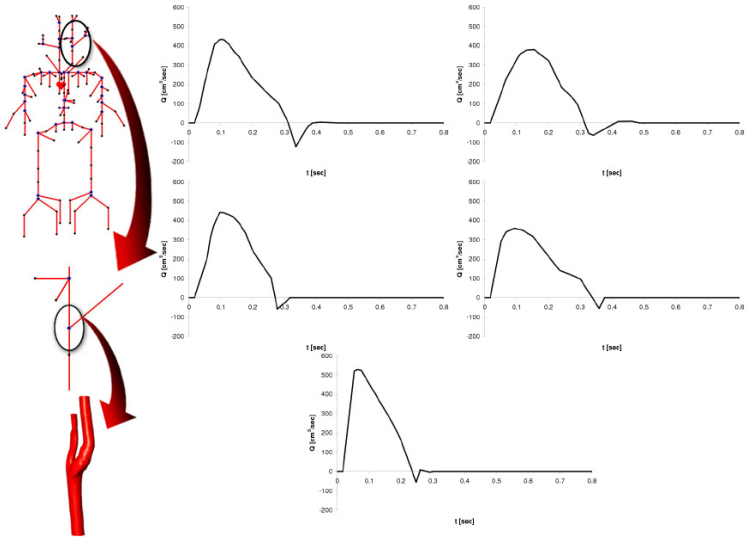

Figure 1: Schematic coupling between 1D / 3D models and 5 heart ejection curves tested. From top to bottom, left to right: Avolio [1], Stergiopulos [3], Spencer [5], a modified version of the Spencer case (which decreases the systolic peak and increases systolic phase) and Stettler [4].

4 RESULTS

Several cardiac cycles were simulated to reach the periodic situation. A non-Newtonian fluid with a Casson law was adopted for the constitutive blood behavior. In the 1D part of the model, time evolution of the flow rate and pressure at the 3D–1D interface corresponding to the common carotid are analyzed. Results for the internal- and external- carotid coupling faces are very similar to this, and therefore were omitted. In the 3D model several comparisons were performed, including the computation of the OSI and WSS indicators since they characterize the oscillating and average behavior of the shear stresses respectively.

Figure 2 clearly shows that the flow rate and the pressure are very sensitive to the inflow boundary conditions in the 1D model. Indeed, the dissimilarities are strongly related to the time derivative of the flow curve before reaching the systolic peak.

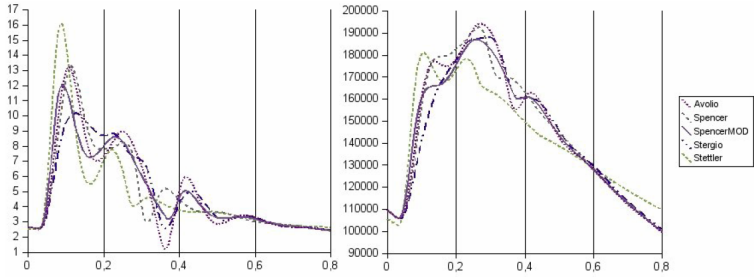

Figure 2: Time evolution of flow rate (left, [cm^3/s]) and pressure (right, [dyn/cm^2]) for the 5 heart ejection curves tested.

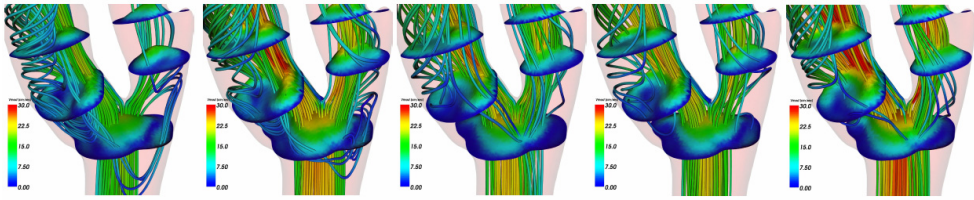

Figure 3: Streamlines and Velocity Profiles for the 5 heart ejection curves tested. From left to right: Avolio (T = 0.365 sec), Spencer (T = 0.315 sec), SpencerMod (T = 0.370 sec), Stergiopulos (T = 0.365 sec) and Stettler (T = 0.280 sec).

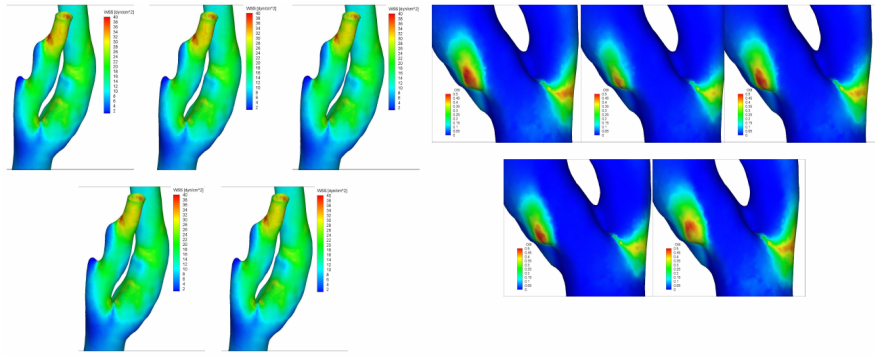

Figure 4: OSI and WSS distributions for the 5 heart ejection curves tested.

Figure 3 shows the streamlines and velocity profiles at the carotid bifurcation at different time instants. Aiming at comparing similar behaviors, data acquisition was made at the last peak in the diastolic phase for all cases, which required to do it at different time instants owing to the differences between the various heart ejection curves tested. Figure 4 shows the distribution of the OSI and WSS indicators respectively. Although the differences observed in the local patterns, no dissimilarities arise between the distribution of the OSI and WSS. This is a straightforward consequence of the low sensitivity of the flow patterns to the cardiac

ejection. Finally, figures 3 and 4 clearly show that the main characteristics of the local flow given by the OSI and WSS, which are averaged quantities along a cardiac cycle, are nearly independent of the inflow boundary condition. Therefore, we infer that when individuals have similar cardiac cycles and similar average flow rates per cardiac cycle, the variability from one subject to another lies mainly in the differences in the geometry of the arterial district.

5 CONCLUSIONS

A numerical study was performed to assess the influence of the heart ejection curve on both local flow patterns and global flow and pressure curves by using a 3D-1D coupled model. Five different curves were tested, all of them having the same period and average flow rate per cardiac period. The response of the 1D model to the different inflow curves varied considerably, which is consistent with the variability found between different subjects. On the other hand, local flow patterns were nearly insensitive to the alteration of the inflow boundary condition. As a result, the computed flow structure indicators did not present significant differences, evidencing the lack of sensitivity of the flow structure to the morphology of the cardiac ejection under the considerations taken in this work. Therefore, we conclude that, while the phenomena occurring at the level of the arterial network is highly dependant upon the cardiac ejection, local phenomena is mainly governed by the geometrical characteristics of the vascular district, always keeping in mind the invariance of the cardiac period and of the average flow rate.

REFERENCES

[1] A.P. Avolio, Multi–branched model of the human arterial system. *Med. Biol. Engrg. Comp*, Vol. 18, pp. 709-718, 1980.

[2] P.J. Blanco, R.A. Feijóo, S.A. Urquiza, A unified variational approach for coupling 3D–1D models and its blood flow applications. *Accepted for publication in Comp. Meth. Appl. Mech. Engrg.*, 2007.

[3] N. Stergiopulos, D.F. Young, T.R. Rogge, Computer simulation of arterial flow with applications to arterial and aortic stenoses. *JB*, Vol. 25, pp. 1477–1488, 1992.

[4] J.C. Stettler, P. Niederer, M. Anliker, Theoretical analysis of arterial hemodynamics including the influence of bifurcations, part I. *Ann. Biomed. Engrg.*, Vol. 9, pp. 145–164, 1981.

[5] M.P. Spencer, A.B. Deninson, The square-wave electro-magnetic flowmeter: theory of operation and design of magnetic probes for clinical and experimental applications. *I.R.E. Trans. Med. Elect.,* Vol. 6, pp. 220-228, 1959.

[6] S.A. Urquiza, P.J. Blanco, M.J. Vénere, and R.A. Feijóo, multidimensional modeling for the carotid blood flow, *Comput. Meth. Appl. Mech. Engrg.*, Vol. 195, pp. 4002–4017, 2006.